TEMPERATURE FIELDS IN LINEAR STAGE OF FRICTION STIR WELDING
Effect of Different Material Properties

by

Darko M. VELJIĆ[a*], Marko P. RAKIN[b], Bojan I. MEDJO[b], Mihailo R. MRDAK[c], and Aleksandar S. SEDMAK[d]

[a] IHIS Science & Technology Park, IHIS Techno Experts Research & Development Center, Belgrade, Serbia
[b] Faculty of Technology and Metallurgy, University of Belgrade, Belgrade, Serbia
[c] IMTEL Communications Ltd., Research and Development Center, Belgrade, Serbia
[d] Faculty of Mechanical Engineering, University of Belgrade, Belgrade, Serbia

Original scientific paper
https://doi.org/10.2298/TSCI181015264V

Friction stir welding is one of the procedures for joining the parts in solid state. Thermo-mechanical simulation of the friction stir welding of high-strength aluminium alloys 2024 T3 and 2024 T351 is considered in this work. Numerical models corresponding to the linear welding stage are developed in Abaqus software package. The material behaviour is modelled by Johnson-Cook law (which relates the yield stress with temperature, strain and strain rate), and the Arbitrary Lagrangian-Eulerian technique is applied. The difference in thermo-mechanical behaviour between the two materials has been analysed and commented. The main quantities which are considered are the temperature in the weld area, plastic strain, as well as the rate of heat generation during the welding process.

Key words: *friction stir welding, finite element model, temperature distribution, heat generation by friction, heat generation by plastic deformation*

Introduction

The friction stir welding (FSW) [1] has found a very wide application in different industry branches, as one of the most efficient procedures for joining the parts in solid state. Its main goal is overcoming the problems characteristic for welding of (primarily aluminium alloys) by melting processes. Most of aluminium alloys can be joined by the application of FSW, but the method is by no means limited to these materials. It has been successfully applied to alloys of nickel, copper, magnesium and titanium, as well as to some steels (typically those with lower strength). Dissimilar joints can also be made, meaning that two different base materials are joined. Applications of this welding procedure are numerous, such as shipbuilding, aerospace, automotive or process industry (vessels for different fluids – hydrogen, oxygen, *etc.*). For example, Boeing applies FSW for the production of fuel tanks for Delta rockets, while Marine Aluminium from Norway uses this technique for joining large parts for ferry boats. Numerous studies of producing and testing of FSW joints can be found in the literature [2-13]. Regarding

* Corresponding author, e-mail: veljic.darko@gmail.com

the joint geometry, butt joints are most often used in practice and analysed in the literature, *e. g.* [6, 7, 11]. However, other joint geometries can also be formed by this welding procedure, such as lap [14, 15] or T-joints [16, 17].

The FSW can generally be split into two stages: plunge and linear welding, fig. 1. The plunge stage initiates the FSW. The tool, which is fabricated from a material with higher hardness in comparison with the welded piece, has two movements in this stage: rotation around its axis and translation in the vertical direction. It penetrates into the plates at the beginning of the joint, establishing the thermo-mechanical conditions which will be maintained during the linear welding stage.

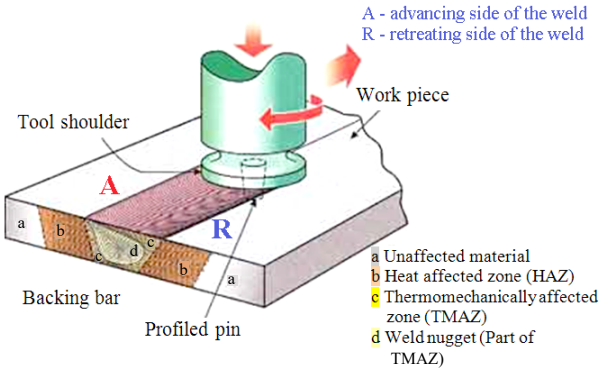

Figure 1. The FSW – tool movement and joint zones (www.twi.co.uk)

After the tool plunge is finished, the tool still rotates around its axis, but the translation has the direction of the joining line. During this movement, the plates are heated due to the friction with the tool, and the material undergoes significant plastic deformation. Softened material flows around the tool pin, and it cools down behind the tool, thus producing the joint. In other words, the welded joint is formed by two actions: heating due to the friction and mechanical deformation due to the rotation of the tool. Energies from both of these sources heat the plates, and the joining occurs at temperatures below the melting point (which is an important property of the FSW).

The heat generation is obtained as a direct transformation of the mechanical energy on the contact surface tool – plates. Therefore, the FSW is a solid state joining process which combines the heat and mechanical work and results in high-quality joints.

As can be seen from the previous description, the FSW is accompanied by high temperatures and plastic flow of the material, which are localised in the vicinity the joining line. Understanding of the material behaviour during the process, [3-7, 9, 11, 14], is beneficial for adequate preparation (parameter selection) and performing of the welding procedure. Another important goal is to prevent the occurrence of defects in produced joints, [15, 18], and minimize the residual stresses [19, 20], both of which can significantly improve the welded structure properties and integrity. Numerical analysis can be of great importance in this context since it provides the values of thermo-mechanical variables (temperature, strain, stress, energy) which can be applied in the optimization of FSW technology, [4-7, 12].

In this work, the influence of material properties on thermo-mechanical quantities (temperature fields, heat generation, reaction force and plastic strain) during FSW is analysed on two very similar materials – aluminium alloys 2024 T3 and 2024 T351.

Materials and methods

Material properties

Both considered materials (alloys 2024 T3 and 2024 T351) have the same chemical composition [8, 21], but their fabrication procedure/processing is different. Accordingly, it can be said that this is the same Al alloy, but subjected to different thermal treatments (*T3 – solution*

heat treated and then cold worked; T351 – solution heat treatment and stress relief by stretching, [21]).

Johnson-Cook expression, [22], is applied for modelling the material behaviour in numerical analysis, eq. (1). The constants which are used for both analysed materials in eq. (1) are given in tab. 1, while basic physical and mechanical material properties can be found in [13, 23].

$$\sigma_y = \left[A + B\cdot\left(\varepsilon_p\right)^n\right]\left[1 + C\left(\frac{\dot{\varepsilon}_p}{\dot{\varepsilon}_o}\right)\right]\left[1 - \left(\frac{T - T_{\text{room}}}{T_{\text{melt}} - T_{\text{room}}}\right)^m\right] \tag{1}$$

Tab. 1. Parameters of the material model [13, 22, 24]

Alloy/ condition	Solidus temp. T_{melt} [°C]	Yield stress A [MPa]	Strain factor B [MPa]	Strain exponent n [–]	Temperature exponent m [–]	Strain rate factor C [–]
2024 T3	502	369	684	0.73	1.7	0.0083
2024 T351	502	265	426	0.34	1	0.015

Finite element model

The model for the linear welding stage is formed with dimensions 100 × 50 × 3 mm, in the software package for finite element analysis Simulia Abaqus (www.simulia.com). Thermo-mechanically coupled hexahedral 8-noded element is used; designation in Abaqus – C3D8RT. It is characterised by linear interpolation for both displacement and temperature, as well as reduced integration [25].

The geometry of the welding tool is given in fig. 2. It can be seen that the pin and the shoulder are cylindrical.

The welding tool and the backing plate (below the welded plate, fig. 2) are modelled as analytical rigid surfaces. They only have mechanical degrees of freedom, *i. e.* their heating is not taken into account. The assembly of all three parts in Abaqus is shown in fig. 3 (there is no mesh on analytical rigid bodies, *i. e.* the tool and the backing plate). More details about the model can be found in [7, 26].

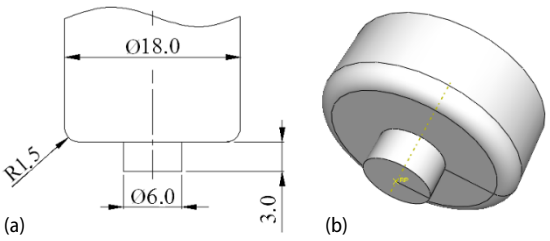

Figure 2. The model of FSW welding tool

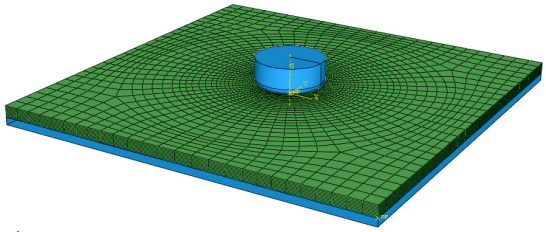

Figure 3. Finite element model (consisting of welding plate, tool and backing plate)

The calculation of the heat generation rate is performed in accordance with the following expressions: $q_p = \eta\tau\dot{\varepsilon}_p$ (component corresponding to plastic deformation) and $\dot{q}_f = \mu p\dot{\gamma}$ (component corresponding to friction between the tool and the welded material). Thermo-mechanical quantities in these equations are shear stress, τ, plastic strain rate, $\dot{\varepsilon}_p$, pressure, p,

and slip rate, $\dot{\gamma}$. The coefficient of friction between the material of the tool and welded plates is μ (value 0.3), while factor η represents the conversion of mechanical to thermal energy (value 0.9), [3]. The heat convection coefficient has the same value on all surfaces of the welding plate, except on the bottom one: $h = 10$ W/m^2°C [3]. The heat is taken from these surfaces by convection (fluid is air, 25 ºC). The h value at the mentioned bottom surface is much higher (3000 W/m^2 °C, [27]), because it takes into account the heat which is taken away through the backing plate.

In a previous paper, [13], heat generation in the same two materials is analysed during the plunge stage, *i. e.* before the linear welding stage is started. Thermo-mechanical analysis of the plunge stage is very important because all thermo-mechanical conditions which are present later during the linear welding are initiated in this stage. The plunging of the tool is characterised by high temperatures (which correspond to hot processing) and extremely pronounced deformation of the material. For the modelling of the plunge stage in [13, 28], thermo-mechanical finite element model with Lagrange formulation is applied, including the remeshing technique.

The linear welding stage presented in this work is modelled, unlike the previously mentioned simulation of the plunge stage, by application of the so-called Arbitrary Lagrangian-Eulerian technique. For the surfaces which are perpendicular to the welding direction, Euler boundary conditions are defined – representing the *inflow* and *outflow* of the material from the model (welding plate). The remaining surfaces of the welding plate are defined as sliding surfaces: side surfaces, top surface (which is in contact with the tool) and bottom surface (which is in contact with the backing plate). Due to the limited possibilities of the mesh adjustment in the Lagrangian-Eulerian technique, the tool pin has a cylindrical shape.

Results and discussion

The temperature field at the beginning of the linear welding stage is given in fig. 4. It is shown on the cross-section, in order to show the values along the thickness. Marked points T1-T4 were used for tracking the temperatures. These points are always in the same position relative to the tool, *i. e.* they move along with the translation of the tool.

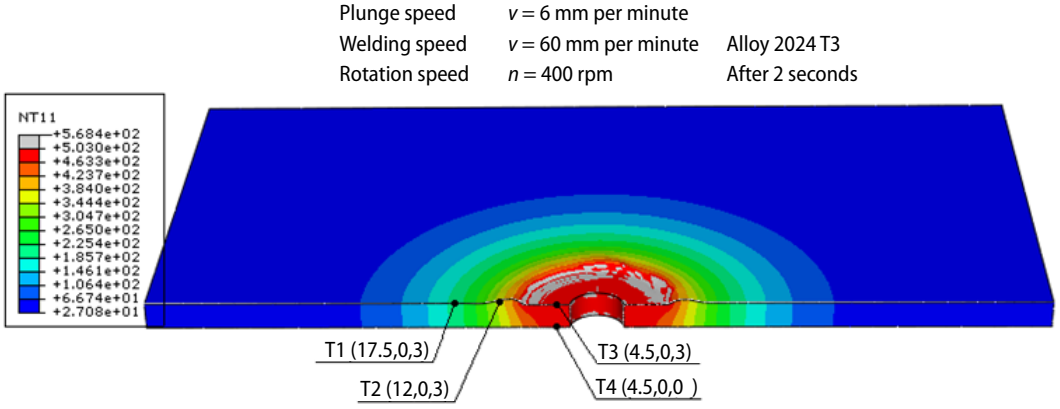

Figure 4. Temperature distribution at the beginning of the welding stage, alloy 2024 T3
(*for color image see journal web site*)

In fig. 5, the rate of heat generation is given for both alloys. It is shown as total energy, as well as decomposed into the parts caused by friction and plastic deformation. The latter is more pronounced for alloy 2024 T3, which can be attributed to higher yield strength and ac-

cordingly higher resistance to deformation. The friction heat generation rate for alloy T3 is somewhat lower because the material is sufficiently heated by plastic deformation, *i. e.* an operating temperature has already been reached in the welding zone and is maintained almost constant.

The total heat generation rate during welding is higher for alloy 2024 T3. The share of heat generation by plastic deformation in total heat generation, when the welding process is steady, for alloy T3 is 40-45% and for alloy T351, 30-35%.

Comparing the diagrams of temperature changes for the same welding parameters, higher temperatures were registered in points T1-T4 for alloy 2024 T3, fig. 6. This is due to intense heat generation for alloy 2024 T3. In fact, in the welding zone operating temperatures are similar for both alloys, but as we approach the periphery of the tool and go on further, the difference is more pronounced.

Heat generation during the FSW is caused by a combination of two different mechanisms: friction between the contact surfaces of the tool and the work-piece (relative sliding of the surfaces) and shear plastic strains in the vicinity of the tool pin and shoulder. In the beginning of the plunging of the tool shoulder into the material, the resistance to this penetration is very high, and the force reaches its maximum. This, in turn, causes an intensive heat generation by friction, which increases the temperature in the welding zone.

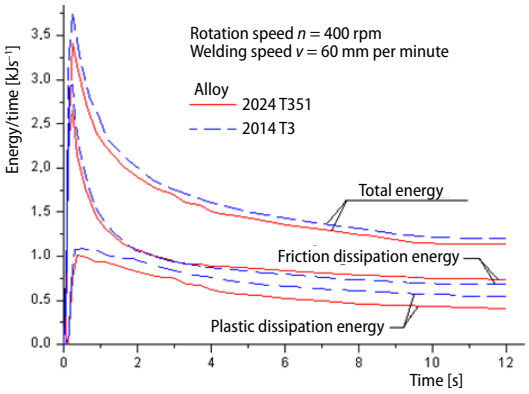

Figure 5. Heat generation due to friction and plastic deformation

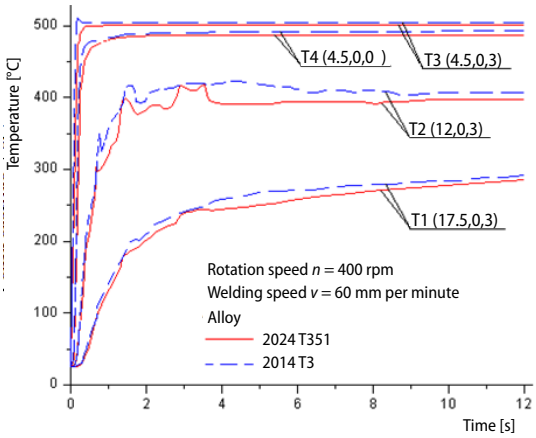

Figure 6. Temperature in measurement points T1-T4

As the temperature for plastic processing of the material is reached, the resistance to tool penetration is decreased. The heat generation by plastic deformation becomes much more intensive, while the friction-generated heat decreases. After 2 seconds, translation of the tool begins, *i. e.* the linear welding is initiated. Soon, the balance between the generated heat and the heat which is *taken away* is established. As a result, the heat generation is approximately constant, as well as temperature and force in the vertical direction, as shown in figs. 5-7 – heat generation approx. 1.25 kJ/s, force in the vertical direction 12-17 kN, temperature on the top surface of the plate under the tool shoulder around 500 °C and temperature on the bottom side of the plate under the tool shoulder around 480 °C

The force in the vertical direction is higher for alloy 2024 T3, *i. e.* this alloy is characterised by higher resistance to deformation, fig. 7.

The equivalent plastic strains for alloy T351 are generally higher, fig. 8, which can mainly be attributed to its lower strength level. Also, the zone with large plastic strain is

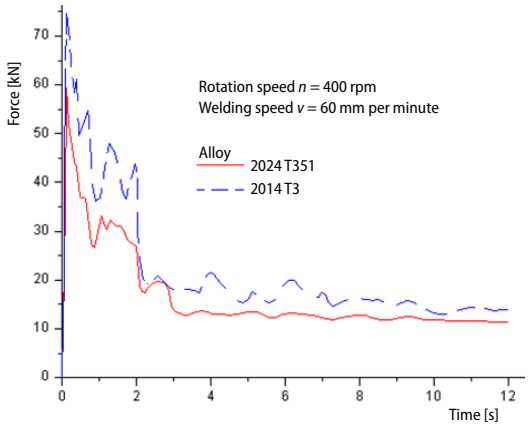

Figure 7. Change of force in the vertical direction

much larger, in all directions, for this alloy. Also, a difference can be seen in the position of the maximum plastic strain. In alloy T3, maximum values are mainly positioned around the tool pin, while two more strain concentration zones are observed in alloy T351 – along the circumference of the tool shoulder and behind the tool on the plate surface.

Different scales are deliberately used in fig. 8, *i. e.* the maximum plastic strain for alloy T3 in the legend is 1%, while for T351 alloy the maximum value is 5%. It is important to emphasize that if the same scale (minimum and maximum plastic strain values) was used, the difference between these figures would be even more pronounced!

Observing the plastic strains on the cross-section of the welded joint, fig. 9, it can be concluded that they are significantly more pronounced at the advancing side for alloy 2024 T351, fig. 9.

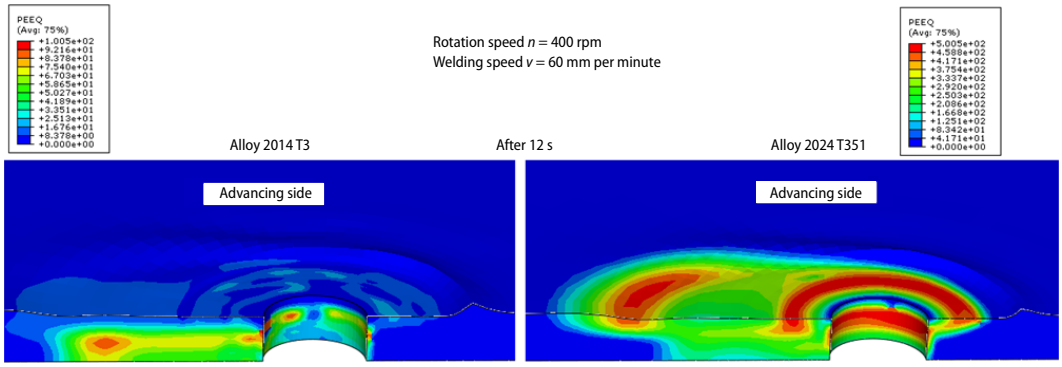

Fig. 8. Equivalent plastic strain distribution (along the joining line)
(*for color image see journal web site*)

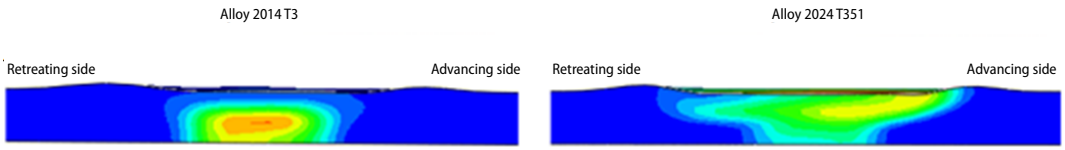

Figure 9. Equivalent plastic strain distribution (joint cross section)
(*for color image see journal web site*)

Conclusions

In this work, the linear welding stage of the friction stir welding process is analysed by the application of the finite element method. Two materials are considered; essentially, it is an aluminium alloy (2024) which has been exposed to different thermal treatments (denotation: 2024 T3 and 2024 T351). Much of the presented results can be related to the heat generation

rate, and there are two main sources of heat in the friction stir welding – intensive plastic deformation of the material around the welding tool and friction between the tool and the material being welded. The results point to a higher rate of heat generation caused by plastic deformation in alloy 2024 T3, while the rate of friction-generated heat is higher for alloy T351. The total heat generation rate during the welding process is higher for alloy T3. Temperatures in the welding zone are similar, but the difference is more pronounced towards the tool periphery. The force in the vertical direction is higher for alloy 2024 T3, while plastic strains are much more pronounced for alloy 2024 T351, as well as the size of the region with high plastic strains.

Acknowledgment

The authors gratefully acknowledge the financial support from the projects TR 34016 and ON 174004 of the Ministry of Education, Science and Technological Development of the Republic of Serbia.

Nomenclature

- h – heat convection coefficient, [$Wm^{-2}\,°C^{-1}$]
- n – rotation speed of the friction stir tool, [rpm]
- v – welding speed, [rpm]
- $\dot{q}_f$ – rate of frictional heat generation, [Js^{-1}]
- $\dot{q}_p$ – rate of heat generation due to plastic energy dissipation, [Js^{-1}]

Greek symbols

- ε_p – equivalent plastic strain, [–]
- $\dot{\varepsilon}_o$ – reference plastic strain rate, [s^{-1}]
- $\dot{\varepsilon}_p$ – equivalent plastic strain rate, [s^{-1}]
- σ_y – current flow stress, [MPa]

References

[1] Thomas, W. M., *et al.*, Improvements Relating to Friction Welding, European Patent EP0653265 A2, 1991.
[2] Mishra, R. S., Mab, Z. Y., Friction Stir Welding and Processing, *Materials Science and Engineering R, 50* (2005), 1-2, pp. 1-78
[3] Schmidt, H., Hattel, J., A Local Model for the Thermomechanical Conditions in Friction Stir Welding, *Modelling & Simulation in Materials Science and Engineering, 13* (2005), 1, pp. 77-93
[4] Song, M., Kovačević, R., Numerical and Experimental Study of the Heat Transfer Process in Friction Stir Welding, *Journal of Engineering Manufacture*, *217* (2003), 1, pp. 73-85
[5] Chen, C. M., Kovačević, R., Finite Element Modelling of Friction Stir Welding - Thermal and Thermomechanical Analysis, *International Journal of Machine Tools & Manufacture*, *43* (2003), 13, pp. 1319-1326
[6] Veljić, D. *et al.*, Numerical Simulation of the Plunge Stage in Friction Stir Welding, *Structural Integrity and Life, 11* (2011), 2, pp. 131-134
[7] Veljić, D. *et al.*, A Coupled Thermo-Mechanical Model of Friction Stir Welding, *Thermal Science, 16* (2012), 2, pp. 527-534
[8] Murariu, A., *et al.* Influence of Material Velocity on Heat Generation During Linear Welding Stage of Friction Stir Welding, *Thermal Science, 20* (2016), 5, pp. 1693-1701
[9] Mijajlović, M. *et al.*, Experimental Studies of Parameters Affecting the Heat Generation in Friction Stir Welding Process, *Thermal Science, 16* (2012), Suppl. 2, pp. 351-362
[10] Živojinović, D., *et al.*, Crack Growth Analysis in Friction Stir Welded Joint Zones using Extended Finite Element Method, *Structural Integrity and Life, 13* (2013), 3, pp. 179-188
[11] Rodriguez, R. I. *et al.*, Microstructure and Mechanical Properties of Dissimilar Friction Stir Welding of 6061-to-7050 Aluminum Alloys, *Materials and Design, 83* (2015), Oct., pp. 60-65
[12] He, X., *et al.*, A Review of Numerical Analysis of Friction Stir Welding, *Progress in Materials Science*, *65* (2014), Aug., pp. 1-66
[13] Veljić, D. *et al.*, Analysis of the Tool Plunge in Friction Stir Welding - Comparison of Aluminum Alloys 2024 T3 and 2024 T351, *Thermal Science, 20* (2016), 1, pp. 247-254
[14] Buffa, G. *et al.*, Friction Stir Welding of Lap Joints: Influence of Process Parameters on the Metallurgical and Mechanical Properties, *Materials Science and Engineering A, 519* (2009), 1-2, pp. 19-26
[15] Song, Y. *et al.*, Defect Features and Mechanical Properties of Friction Stir Lap Welded Dissimilar AA2024-AA7075 Aluminum Alloy Sheets, *Materials and Design, 55* (2014), Mar., pp. 9-18

[16] Silva, A. *et al.*, Friction stir welded T-joints optimization, *Materials and Design, 55* (2014), Mar., pp. 120-127
[17] Živković, A. *et al.*, Friction Stir Welding of Aluminium Alloys - T Joints, *Structural Integrity and Life, 15* (2015), 3, pp. 181-186
[18] Kah, P. *et al.*, Investigation of Weld Defects in Friction-Stir Welding and Fusion Welding of Aluminium Alloys, *International Journal of Mechanical and Materials Engineering, 10* (2015), 1, paper no. 26
[19] Hattel, J. H. *et al.*, Modelling Residual Stresses in Friction Stir Welding of Al Alloys – A Review of Possibilities and Future Trends, *International Journal of Advanced Manufacturing Technology, 76* (2015), 9, pp. 1793-1805
[20] Zapata, J. *et al.*, Residual Stresses in Friction Stir Dissimilar Welding of Aluminum Alloys, *Journal of Materials Processing Technology, 229* (2016), Mar., pp. 121-127
[21] ***, Certificate conformity, ALCOA International, Inc, Approved Certificate No. 47831, 1990
[22] Johnson, G. R., Cook, W. H., A Constitutive Model and Data for Metals Subjected to Large Strains, High Rates and High Temperatures, *Proceedings*, 7th International Symposium on Ballistics, The Hague, The Netherlands, 1983, pp. 541-547
[23] ***, ASM International Aluminum 2024-T351 Data Sheet, http://asm.matweb.com/search/SpecificMaterial.asp?bassnum=MA2024T4
[24] Lesuer, D. R., Experimental Investigations of Material Models for Ti-6Al-4V Titanium and 2024-T3 Aluminium, Final Report, Department of Transportation, Washington DC, USA, 2000
[25] ***, Dassault Systemes, Abaqus Analysis Manual, 2011
[26] Veljić, D. *et al.*, Experimental and Numerical Thermo – Mechanical Analysis of Friction Stir Welding of High – Strength Alluminium Alloy, *Thermal Science, 18* (2014), Suppl. 1, pp. S29-S38
[27] Park, K., Development and Analysis of Ultrasonic Assisted Friction Stir Welding Process, Ph. D. thesis, University of Michigan, Ann Arbor, Mich., USA, 2009
[28] Veljić, D. *et al.*, Heat Generation during Plunge Stage in Friction Stir Welding, *Thermal Science, 17* (2013), 2, pp. 489-496

Paper submitted: October 15, 2018
Paper revised: May 31, 2019
Paper accepted: May 31, 2019